

Investigating radial flow-like effects via pseudorapidity and transverse sphericity dependence of particle production in pp collisions at the LHC

Aswathy Menon Kavumpadikkal Radhakrishnan¹, Suraj Prasad¹,
Sushanta Tripathy², Neelkamal Mallick¹, and Raghunath Sahoo^{1*}

¹*Department of Physics, Indian Institute of Technology Indore, Simrol, Indore 453552, India and*

²*CERN, Geneva 23 1211, Switzerland*

(Dated: February 11, 2025)

Recent observations of quark-gluon plasma (QGP) like signatures in high multiplicity proton-proton (pp) collisions, have compelled the heavy-ion physics community to re-examine small collision systems for proper baseline studies. Event-shape-based studies in pp collisions have succeeded to a certain extent in identifying the rare events mimicking such heavy-ion-like behaviour. In this study, we incorporate PYTHIA8 and AMPT to study radial flow-like signatures in pp collisions at $\sqrt{s} = 13$ TeV as a function of transverse sphericity and pseudorapidity. The selection of softer events possibly carrying heavy-ion-like features is performed using the transverse sphericity event-shape observable. As the particle production mechanism in midrapidity differs greatly from the forward rapidity, a pseudorapidity-dependent study is meaningful. Keeping ALICE 3 upgrades at the LHC in mind, this study aims to demonstrate the transverse sphericity and pseudorapidity dependence of the mean transverse momentum, particle ratios, and kinetic freezeout parameters in pp collisions at $\sqrt{s} = 13$ TeV using PYTHIA8. We observe that the isotropic events show enhanced radial-flow effects in all multiplicity classes, however, the jetty events show signatures of the radial flow-like effects only in high-multiplicity events. For the first time, we show the transverse sphericity and pseudorapidity dependence of partonic modification factor in pp collisions, which clearly shows that by choosing transverse sphericity, one can directly probe the radial flow-like effects in pp collisions at the LHC.

I. INTRODUCTION

One of the primary goals of heavy-ion collisions at ultra-relativistic energies is to probe the quantum chromodynamics (QCD) phase diagram. Such collisions at the Large Hadron Collider (LHC) and Relativistic Heavy-Ion Collider (RHIC) form a state of deconfined partons in thermal equilibrium called the quark-gluon plasma (QGP), which is believed to have existed a few microseconds after the Big Bang. It is nearly impossible to directly observe such a deconfined medium in heavy-ion collisions due to its short lifetime. However, there are a few indirect signatures that can signify the presence of such a medium. These QGP-signatures require a non-QGP baseline measurement to compare with. Traditionally, proton-proton (pp) collisions have been used as the baseline to study these signatures for last few decades; however, recent observations of ridge-like structures [1, 2], observation of strangeness enhancement [3] and radial flow-like signatures [4–6] in high multiplicity pp collisions have impelled the scientific community to re-examine the origin of such heavy-ion-like features in small collision systems.

In hydrodynamical models of heavy-ion collisions, the radial flow is believed to give a boost to the particles based on their transverse momentum (p_T), where higher momentum particles get a greater boost compared to the lower momentum particles for a given particle species. This p_T -dependent boost due to radial flow gives rise to

the broadening of the p_T -spectra of the particle, thus enhancing mean transverse momenta. The broadening also depends on the particle mass as particles with lower mass are less affected in the presence of radial flow as compared to the particles with higher mass [7]. This difference in broadening of transverse momentum spectra for particles of different masses leads to a peak-like structure around 2-3 GeV/c in transverse momentum in the ratios of particle yields for different masses. In Pb–Pb collisions, the central collisions are observed to have more such radial flow effect compared to the peripheral collisions [8]. In contrast, kinetic theory-based models such as a multi-phase transport model (AMPT) are able to explain many of the experimental features of particle spectra and flow [9–18]. It includes radial and anisotropic flow, which provides crucial information on the collectivity of the system formed in heavy-ion collisions. Both elliptic and triangular flow from AMPT qualitatively explain the experimental results [11–15]. In Refs. [12, 13], the authors study the number of constituent quark (NCQ) scaling of elliptic flow using AMPT, where a qualitative agreement between experiment and models can be observed.

However, perturbative quantum chromodynamics (pQCD) inspired models such as PYTHIA [19] with the implementation of color reconnection (CR) and multi-partonic interactions (MPI) are seen to be capable of imitating the radial flow-like effects in pp collisions [20–22]. These radial flow-like effects in pp collisions using PYTHIA8 are shown to have a positive correlation with the number of multi-partonic interactions (N_{mpi}). Events with a higher value of N_{mpi} can mimic enhanced radial flow-like effects [23] as compared to events with low N_{mpi} .

* Corresponding author: raghunath.sahoo@cern.ch

In experiments, it is impossible to measure N_{mpi} directly. However, event shape-based study using transverse sphericity is one such method to probe N_{mpi} as the correlation between transverse sphericity and N_{mpi} is found to be significant in simulations. Transverse sphericity, being an event-shape observable, is capable of separating the events based on their geometrical shapes [24]. It can identify the soft-QCD-dominated isotropic events and the hard-QCD-dominated jetty events. This feature of transverse sphericity makes it a perfect tool for studying the emerging QGP-like signatures in small collision systems with special interest to the high N_{mpi} events [24–32].

The particle production mechanism in high-energy nuclear and hadronic collisions can be affected by different effects, such as nuclear modification of partonic distribution function, multiple partonic scattering, possible parton saturation and radial flow, where these effects are expected to depend upon pseudorapidity and charged particle multiplicity of the produced hadrons [4, 33–36]. A few studies on pseudorapidity dependence of particle production have been performed at the LHC [33, 34, 37–39], and RHIC [40–44]. In Ref. [40], the study of mean transverse radial flow velocity ($\langle\beta_{\text{T}}\rangle$) and the kinetic freeze-out temperature (T_{kin}) extracted from the simultaneous Boltzmann Gibbs blastwave function fit of the identified particles’ p_{T} -spectra in Cu–Cu collisions at $\sqrt{s_{\text{NN}}} = 200$ GeV shows a rapidity dependence. Here, $\langle\beta_{\text{T}}\rangle$ decreases towards the forward rapidity regions. This could be due to the availability of lower energy (and hence lower $\langle p_{\text{T}}\rangle$) in the system at forward rapidity. In addition, using a multi-phase transport model in Pb–Pb collisions at LHC energies, both $\langle\beta_{\text{T}}\rangle$ and T_{kin} are found to have a transverse sphericity dependence, indicating that the isotropic events can have more radial flow compared to the jetty events [32, 45]. The studies mentioned above signify the importance of pseudorapidity and event-shape dependence of particle production in pp, p–Pb and Pb–Pb collisions. Thus, a systematic study of event-shape and pseudo-rapidity dependence of particle production in small collision systems can enable the scientific community to unveil the physical processes contributing to the observed heavy-ion-like phenomena in pp and p–Pb collisions [33].

In this study, we employ transverse sphericity as an event shape observable to study the pseudorapidity dependence of radial flow-like effects in pp collisions at $\sqrt{s} = 13$ TeV. We report observables sensitive to radial flow-like effects such as the mean transverse momentum, particle ratios, and kinetic freezeout parameters as a function of transverse sphericity and pseudorapidity. For this study, we use PYTHIA8, which explains the experimentally observed flow-like effects with good qualitative agreement and can provide a clear effect of MPI activity in different rapidity regions. A comparison with a multi-phase transport model is also shown for specific cases, which can help to make a model-independent agreement on the dependence of transverse sphericity and pseudorapidity on the reported observables. Another crucial

point is that transverse sphericity is usually defined in the midrapidity ($|\eta| < 0.8$) due to the current constraints of charged-particle measurement in the forward pseudorapidity at the LHC. However, with upcoming ALICE 3 upgrades, one can make measurements with particle identification for a wider pseudorapidity coverage, i.e., $|\eta| < 4.0$ [46]. Thus, keeping ALICE 3 upgrades at the LHC in mind, this study aims to demonstrate the sphericity and pseudorapidity dependence of a few observables. Consequently, we define the transverse sphericity in a broader range of pseudorapidity *i.e.* $S_0(|\eta| < 2.0)$.

The paper is organized as follows. We start with an adequate introduction in Sec. I, then discuss the event generation using PYTHIA8 and AMPT as well as transverse sphericity in Sec. II, and later discuss the observables, and results in Sec. III. Finally, we summarise our findings in Sec. IV.

II. EVENT GENERATION AND METHODOLOGY

In this section, we discuss the event generation model, specific tunes, and analysis methodology. We start the description with the pQCD-inspired PYTHIA8 model and kinetic-theory based AMPT model. We then discuss transverse sphericity, which is the event-shape observable.

A. PYTHIA8

PYTHIA is a widely used perturbative QCD-inspired Monte Carlo event generator to simulate hadronic, leptonic, and heavy-ion collisions with emphasis on physics related to small collision systems like pp collisions [19]. PYTHIA8 involves soft and hard QCD processes and contains the models for initial and final state parton showers, multiple parton-parton interactions, beam remnants, string fragmentation, and particle decays. In our present study, we have implemented the default 4C tune of PYTHIA8 (version 8.308) with the MPI and CR mechanisms involving soft-QCD processes and hadronic decays [47, 48]. The particles originating from the MPIs and the beam remnants form the underlying event. The Lund string fragmentation model performs the hadronisation of these partons [47]. The CR picture makes sure that the string between the partons is arranged in such a way that the total string length is reduced, which in turn leads to reduced particle multiplicity of the event. The 4C tune [48] based on MPI and CR is able to reproduce many features of the experimental pp collisions data reasonably well [20, 21].

B. A multi-phase transport model (AMPT)

AMPT is a kinetic theory-based model and possesses four main components as follows [49–65].

1. Initialisation of collisions: The collisions in the AMPT model are initialized by HIJING where the production cross-sections of mini-jet partons and excited strings are calculated for pp collisions [61].
2. Parton transport: In the default version of AMPT, the produced minijet partons are transported through Zhang’s parton cascade model [62]. In the string melting version, excited strings also participate in Zhang’s parton cascade.
3. Hadronisation: In the default version of AMPT, the transported partons are hadronized using the Lund string fragmentation model. In the string melting version, the quark coalescence mechanism is used for the hadronization of the transported partons [55, 63].
4. Hadron Transport: The produced hadrons are transported through meson-meson, meson-baryon, and baryon-baryon interactions using a relativistic transport model [64, 65].

The string-melting mode of AMPT is able to reproduce many of the experimental features of particle flow and p_T -spectra [66, 67]. In this study, we use the string melting mode of AMPT (version 2.26t9b). We use the Lund symmetric splitting function parameters as $a = 0.5$ and $b = 0.9$ to match the experimental p_T -spectra. In addition, the parton cross-section is set to 3 mb with a parton screening mass of 2.265 fm^{-1} and alpha in the parton cascade as 0.33. All other settings of AMPT are kept the same as in Ref. [68]. With these settings in AMPT, we simulate pp collisions at $\sqrt{s} = 13 \text{ TeV}$ for this study.

Figure 13 (in the appendix) shows the comparison of the above-mentioned tunes of PYTHIA8 with the AMPT and ALICE measurements from Ref. [69] for p_T -spectra of minimum bias pp collisions at $\sqrt{s} = 13 \text{ TeV}$. As shown, the PYTHIA8-based 4C tune overestimates the experimental data, where it keeps a good qualitative agreement with the experimental measurements within 10% uncertainties. On the other hand, the p_T -spectra from AMPT underestimate the experimental curve, where it gives a good description only in the intermediate to high p_T region.

C. Transverse Sphericity

Transverse sphericity is a well-established event shape classifier in pp collisions, capable of separating the pQCD dominated hard events from the soft-QCD events. It is also observed that the selections based on the transverse

sphericity, indeed, can identify the events with enhanced production of strange hadrons [70], similar to radial flow effects [28] in pp collisions.

Transverse sphericity, an infrared and co-linear safe quantity, is defined for a unit vector $\hat{n}(n_T, 0)$ in the transverse plane as [24],

$$S_0 = \frac{\pi^2}{4} \min_{\hat{n}} \left(\frac{\sum_{i=1}^{N_{\text{had}}} |\mathbf{p}_T \times \hat{n}|}{\sum_{i=1}^{N_{\text{had}}} |\mathbf{p}_T|} \right)^2 \quad (1)$$

Here, \hat{n} is chosen such that the ratio within parenthesis is minimized for a given event. The summations run over all the charged hadrons in an event, and N_{had} is the total number of charged hadrons. Multiplication of $\pi^2/4$ in Eq. 1 makes S_0 to lie between 0 and 1. The extreme limits of S_0 represent specific configurations of the produced particles on the transverse plane. The lower limit of transverse sphericity ($S_0 \rightarrow 0$) characterizes hard jetty events with back-to-back (pencil-like) emission of particles, while the higher limit ($S_0 \rightarrow 1$) corresponds to soft isotropic events. In this study, transverse sphericity is determined using the charged hadrons in the pseudo-rapidity range, $|\eta| < 2.0$ having transverse momentum, $p_T > 0.15 \text{ GeV}/c$. We restrict our estimations of transverse sphericity only to the events having more than 5 charged hadrons within the mentioned kinematic region. The jetty and isotropic event classes are categorised by choosing transverse sphericity cuts corresponding to the lowest 20% and highest 20% events in the sphericity distribution, respectively. For the sake of simplicity, we may conveniently replace transverse sphericity as sphericity throughout the remaining text.

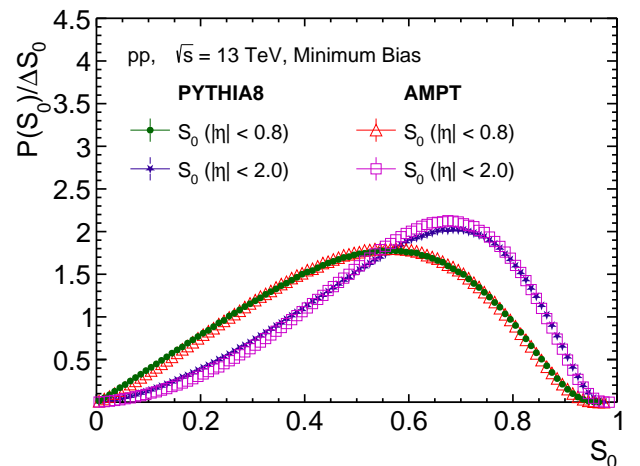


FIG. 1. (Color online) Transverse sphericity distribution ($S_0(|\eta| < 0.8)$ and $S_0(|\eta| < 2.0)$) in pp collisions at $\sqrt{s} = 13 \text{ TeV}$ using PYTHIA8 and AMPT.

Figure 1 compares the transverse sphericity distributions for minimum bias pp collisions at $\sqrt{s} = 13 \text{ TeV}$ using PYTHIA8 as well as AMPT with two kinematics

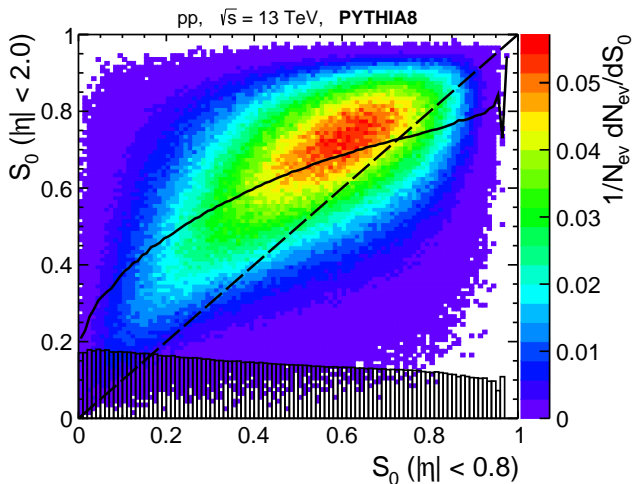


FIG. 2. (Color online) Correlation between S_0 measured in $|\eta| < 0.8$ and $|\eta| < 2.0$ in pp collisions at $\sqrt{s} = 13$ TeV using PYTHIA8. The solid line represents the average value of the y -axis at a particular value of x -axis and the dashed line guides $S_0(|\eta| < 0.8) = S_0(|\eta| < 2.0)$. The bar representation in the figure shows the standard deviation value of the y -axis for each bin in x -axis.

cuts, one with sphericity defined for the particle tracks in the conventional pseudorapidity range, $|\eta| < 0.8$ and the other one with the sphericity in the pseudorapidity range $|\eta| < 2.0$. Here, the peak of S_0 distribution is shown to be shifted to a higher sphericity limit as we widen the rapidity region for transverse sphericity from $|\eta| < 0.8$ to $|\eta| < 2.0$ for both PYTHIA8 and AMPT simulations. The shift of the $S_0(|\eta| < 2.0)$ distribution to the right as compared to the $S_0(|\eta| < 0.8)$ curve is attributed to the inclusion of softer particles (low p_T) as we move to a wider pseudorapidity range. In addition, it is also interesting to note that the transverse sphericity distribution for both $|\eta| < 0.8$ and $|\eta| < 2.0$ from PYTHIA8 matches the distributions from AMPT quite well.

Figure 2 shows the correlation between two definitions of sphericity, *i.e.*, between $S_0(|\eta| < 0.8)$ and $S_0(|\eta| < 2.0)$ from PYTHIA8; the solid line represents the average value of y -axis at a particular value of x -axis. The figure pictorially represents the shift in the sphericity values after the inclusion of a wider pseudorapidity region, *i.e.*, from $|\eta| < 0.8$ to $|\eta| < 2.0$, for the estimation of sphericity. As one notices, the region above the $x = y$ line for $S_0(|\eta| < 0.8) < 0.7$ is largely populated. This indicates that majority of events having $S_0(|\eta| < 0.8) < 0.7$ acquire a larger $S_0(|\eta| < 2.0)$ value. On the other hand, the events having $S_0(|\eta| < 0.8) > 0.7$ largely populate the region below $x = y$ line; however, the shift of mean and variance of $S_0(|\eta| < 2.0)$ is small compared to the events having $S_0(|\eta| < 0.8) < 0.7$. This fairly indicates that the isotropic events are less affected by the change of the pseudorapidity window in the definition of transverse sphericity as compared to the jetty events.

Figure 3 shows the correlation between average trans-

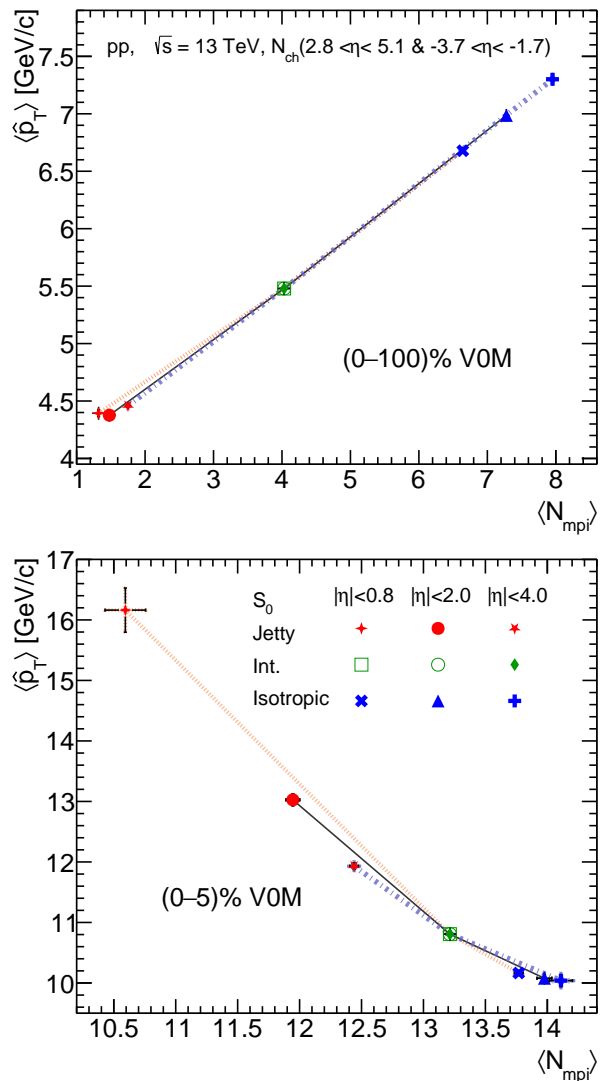


FIG. 3. (Color online) Correlation between $\langle \hat{p}_T \rangle$ and $\langle N_{\text{mpi}} \rangle$ as a function of $S_0(|\eta| < 0.8)$, $S_0(|\eta| < 2.0)$ and $S_0(|\eta| < 4.0)$ in (0-100)% VOM (upper) and (0-5)% VOM (lower) in pp collisions at $\sqrt{s} = 13$ TeV using PYTHIA8.

verse momentum transfer of the hardest parton-parton interaction ($\langle \hat{p}_T \rangle$) and average number of multi-partonic interactions ($\langle N_{\text{mpi}} \rangle$) as a function of $S_0(|\eta| < 0.8)$, $S_0(|\eta| < 2.0)$ and $S_0(|\eta| < 4.0)$ in (0-100)% (upper) and (0-5)% (lower) VOM classes in pp collisions at $\sqrt{s} = 13$ TeV using PYTHIA8. For (0-100)% VOM case, one finds a linear correlation between $\langle N_{\text{mpi}} \rangle$ and $\langle \hat{p}_T \rangle$. Here, $\langle \hat{p}_T \rangle$ increases as one goes to isotropic events with increasing $\langle N_{\text{mpi}} \rangle$. However, for (0-5)% VOM class, which is dominated by both soft processes and multi-jet topologies leading to higher multiplicity, one finds an anti-correlation between $\langle N_{\text{mpi}} \rangle$ and $\langle \hat{p}_T \rangle$ as a function of transverse sphericity selection [71, 72]. $S_0(|\eta| < 4.0)$ is found to isolate events with large $\langle N_{\text{mpi}} \rangle$ in both (0-100)% and (0-5)% VOM classes. On the other hand, $S_0(|\eta| < 0.8)$ is limited with a smaller value of $\langle N_{\text{mpi}} \rangle$ in

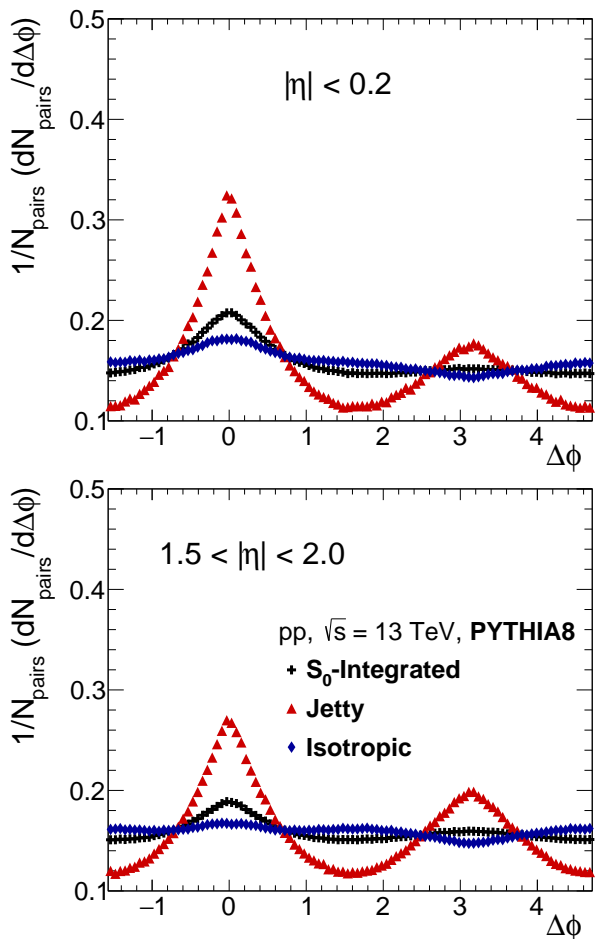


FIG. 4. (Color online) Sphericity dependence of $\Delta\phi$ distributions for charged-particles in $|\eta| < 0.2$ (top) and $1.5 < |\eta| < 2.0$ (bottom) for (0 – 100)% V0M class in pp collisions at $\sqrt{s} = 13$ TeV using PYTHIA8.

V0M Percentile	$\langle dN_{\text{ch}}/d\eta \rangle_{ \eta < 2.0}$	$S_0(\eta < 2.0)$ range	
		Jetty	Isotropic
0 – 1	25.323 ± 0.017	0 - 0.675	0.865 - 1
1 – 5	20.074 ± 0.007	0 - 0.645	0.845 - 1
5 – 10	16.427 ± 0.006	0 - 0.615	0.835 - 1
10 – 20	12.903 ± 0.004	0 - 0.585	0.815 - 1
20 – 30	9.550 ± 0.003	0 - 0.535	0.795 - 1
30 – 40	7.054 ± 0.003	0 - 0.485	0.765 - 1
40 – 50	5.091 ± 0.002	0 - 0.425	0.735 - 1
50 – 70	3.377 ± 0.001	0 - 0.355	0.695 - 1
0 – 100	6.702 ± 0.002	0 - 0.425	0.765 - 1

TABLE I. Transverse sphericity cuts for the jetty and isotropic events for different multiplicity classes in pp collisions at $\sqrt{s} = 13$ TeV using PYTHIA8.

the isotropic events as compared to the other two definitions of transverse sphericity. In contrast, the advantage

V0M Percentile	$\langle dN_{\text{ch}}/d\eta \rangle_{ \eta < 2.0}$	$S_0(\eta < 2.0)$ range	
		Jetty	Isotropic
0 – 1	25.780 ± 0.018	0 - 0.662	0.858 - 1
1 – 5	19.792 ± 0.008	0 - 0.632	0.844 - 1
5 – 10	15.480 ± 0.006	0 - 0.600	0.828 - 1
10 – 20	11.472 ± 0.004	0 - 0.556	0.808 - 1
20 – 30	8.310 ± 0.003	0 - 0.512	0.786 - 1
30 – 40	6.368 ± 0.002	0 - 0.478	0.766 - 1
40 – 50	4.907 ± 0.002	0 - 0.446	0.748 - 1
50 – 70	3.600 ± 0.001	0 - 0.402	0.722 - 1
0 – 100	6.476 ± 0.002	0 - 0.435	0.765 - 1

TABLE II. Transverse sphericity cuts for the jetty and isotropic events for different multiplicity classes in pp collisions at $\sqrt{s} = 13$ TeV using AMPT.

of using $S_0(|\eta| < 2.0)$ as an event shape classifier is that it can probe events with higher $\langle N_{\text{mpi}} \rangle$ as compared to $S_0(|\eta| < 0.8)$, and is better at isolating hard events as compared to $S_0(|\eta| < 4.0)$.

In this study, the charged particle multiplicity selection is made in the V0 detector acceptance region (V0M) of the ALICE experiment at the LHC, *i.e.*, $-3.7 < \eta < -1.7$ and $2.8 < \eta < 5.1$ [73]. The percentile cuts for the corresponding V0M selection from PYTHIA8 and AMPT are listed in the first column of Tab. I and Tab. II respectively. In addition, the table includes corresponding mean charged particle density measured in the mid-rapidity region, *i.e.*, $|\eta| < 2.0$ along with the sphericity cuts for jetty and isotropic events in each V0M class. Here, the differential study for pseudorapidity is performed in six pseudorapidity regions, *viz.*, $|\eta| < 0.2$, $0.2 \leq |\eta| < 0.4$, $0.4 \leq |\eta| < 0.7$, $0.7 \leq |\eta| < 1$, $1 \leq |\eta| < 1.5$ and $1.5 \leq |\eta| < 2$. From Figs. 1, 2, and 3, it is evident that the sphericity estimated with a wider pseudorapidity cut behaves qualitatively similar to the midrapidity definition, and therefore, sphericity estimated with $|\eta| < 2.0$ can be taken as the standard definition for the rest of results mentioned in this study. Exceptions, if any, shall be mentioned in the respective cases. The choice to widen the η range for the estimation of S_0 for this particular study is only because this work aims to study the pseudorapidity dependence of radial flow-like effects. However, we do not compare the results obtained from the event-shape selection with the two definitions of transverse sphericity.

Finally, the event selection capability of sphericity, $S_0(|\eta| < 2.0)$, for the jetty and isotropic events, can be evaluated by studying the relative azimuthal angle ($\Delta\phi$) distribution of all the charged particles with respect to the highest p_T charged hadron known as the trigger, which is calculated as $\Delta\phi = \phi_{\text{trig.}} - \phi_{\text{track.}}$ Figure 4 shows the $\Delta\phi$ distributions for the charged-particles in two different pseudorapidity cuts, *i.e.*, in $|\eta| < 0.2$ and $1.5 < |\eta| < 2.0$, by considering the triggers in the respec-

tive η -cuts in (0–100)% V0M class from PYTHIA8. The jetty and isotropic event selections are performed using $S_0(|\eta| < 2.0)$ for both plots. The plots are normalized by dividing the number of particle pairs (N_{pairs}) in the respective η ranges. In both the pseudorapidity cases, the jetty events show larger near and away side peaks and the isotropic events show an almost flat (symmetric) distribution of particles in $\Delta\phi$ as compared to the S_0 -integrated events. The presence of clear jet peaks in jetty events and a flat distribution in isotropic events in both the η -cuts, signify that the capability of sphericity to disentangle the jetty and isotropic events remains intact, and hence, it is a suitable candidate for the event selection as well as the study of pseudorapidity dependent properties of various observables which are described in the next section.

III. RESULTS AND DISCUSSIONS

In this section, we present the results of some of the observables, such as particle ratios, partonic modification factor, mean transverse momentum, kinetic freezeout properties, and transverse momentum crossing points, which are believed to be sensitive to the radial flow effects.

A. Particle ratios

The hydrodynamic expansion of the hot and dense partonic medium formed in the collisions of nuclear matter creates an azimuthally symmetric and radially outward flow of the particles known as the radial flow. Thus, the presence of radial flow hints towards the formation of QGP and hence, the applicability of hydrodynamics as the local thermal equilibrium of the medium is achieved. This radial flow is expected to give a larger boost to the particles with higher mass compared to the lower mass. As the massive particles gain more momentum from the flow velocity, the observed broadening in p_T spectra is expected to be different for particles from low to high masses. This mass ordering in the degree of broadening of p_T spectra signals the presence of radial flow in the system. In Ref. [7], authors have explicitly discussed the effect of radial flow for different particles. It has been observed that the p_T spectra of pions, in the presence of a strong radial flow, acquire a ‘convex’ shape while protons develop a positive curvature. In the presence of radial flow, the slopes of the p_T spectra of all particles become less steep. This mass-dependent modification in the particle p_T spectra in the presence of radial flow can also be seen in the p_T -dependent yield ratios of different particles. For a radially boosted system, a bump-like structure is observed in the particle yield ratios in the intermediate p_T region. This bump-like structure shifts to a higher p_T value for a more radially boosted system [74, 75]. In Pb–Pb collisions at TeV energies, the

proton-to-pion ratio exhibits strong enhancement (bump-like structure) in the intermediate p_T region compared to pp collisions [8, 74, 75]. In addition, as one moves from central to peripheral collisions, this enhancement structure in the particle yield ratio shifts towards the lower p_T values. Radial flow is known to depend on the centrality and it decreases as one moves from the central to the peripheral collisions and hence, the shift of the bump-like structure from intermediate to low p_T is observed [8, 74, 75].

Recently, such radial flow-like signals in the particle yield ratios are observed in high multiplicity pp collisions [4, 5], which are otherwise taken as the baseline measurement system without QGP, for the comparison with heavy-ion collisions. Interestingly, PYTHIA8, a pQCD inspired model, can mimic the signatures of radial flow with color reconnection. As mentioned in Ref. [21], in PYTHIA8, a string that connects two partons follows the movements of the partonic endpoints, leading to a common boost of the string fragments (hadrons). In the absence of CR, when a parton is knocked out in the midrapidity, the other string end will be part of the proton moving forward, leading to a small boost. However, in the presence of CR, two partons from independent hard scatterings at similar rapidity can color reconnect and make a large transverse boost. In the presence of CR, with an increase in N_{mpi} , the partonic collisions increase, thus the boost further increases, which consequently mimics the hydrodynamical radial flow. Although, in PYTHIA8, the source of such an observation is clearly different from hydrodynamics, PYTHIA8 mimics the features of radial flow very well. Thus we may call these features of PYTHIA8, which mimic the hydrodynamical radial flow as “radial flow-like effects”.

In this section, we try to investigate the sphericity and pseudorapidity dependence of proton to pion yield ratio in pp collisions at $\sqrt{s} = 13$ TeV. For simplicity, we denote $(p + \bar{p})/(\pi^+ + \pi^-)$ as p/π . The top panel in each of the four plots in Fig 5 shows p/π as a function of transverse momentum in $|\eta| < 2.0$ for the jetty, S_0 -integrated, and isotropic events using PYTHIA8 (left plots) and AMPT (right plots) while the bottom panel shows the ratio of p/π of the jetty and isotropic events to that of the S_0 -integrated events. The upper plots corresponds to the (0 – 100)% V0M multiplicity class whereas the bottom plots are for the high-multiplicity pp collisions, i.e., (1 – 5)% V0M class. For both the multiplicity classes, using the CR mode in PYTHIA8, the S_0 -integrated events show a clear peak in the intermediate p_T . This peak-like structure appearing in the p/π is attributed to color reconnection in PYTHIA8 [20, 21], which is analogous to the peaks in the p/π of Pb–Pb collisions due to the hydrodynamical radial flow. Also, for both the multiplicity classes shown here, the p/π for the isotropic events show a larger peak in the intermediate p_T as compared to the S_0 -integrated case. This clearly hints that for isotropic events having a large value of N_{mpi} , radial flow-like effects are enhanced. As expected,

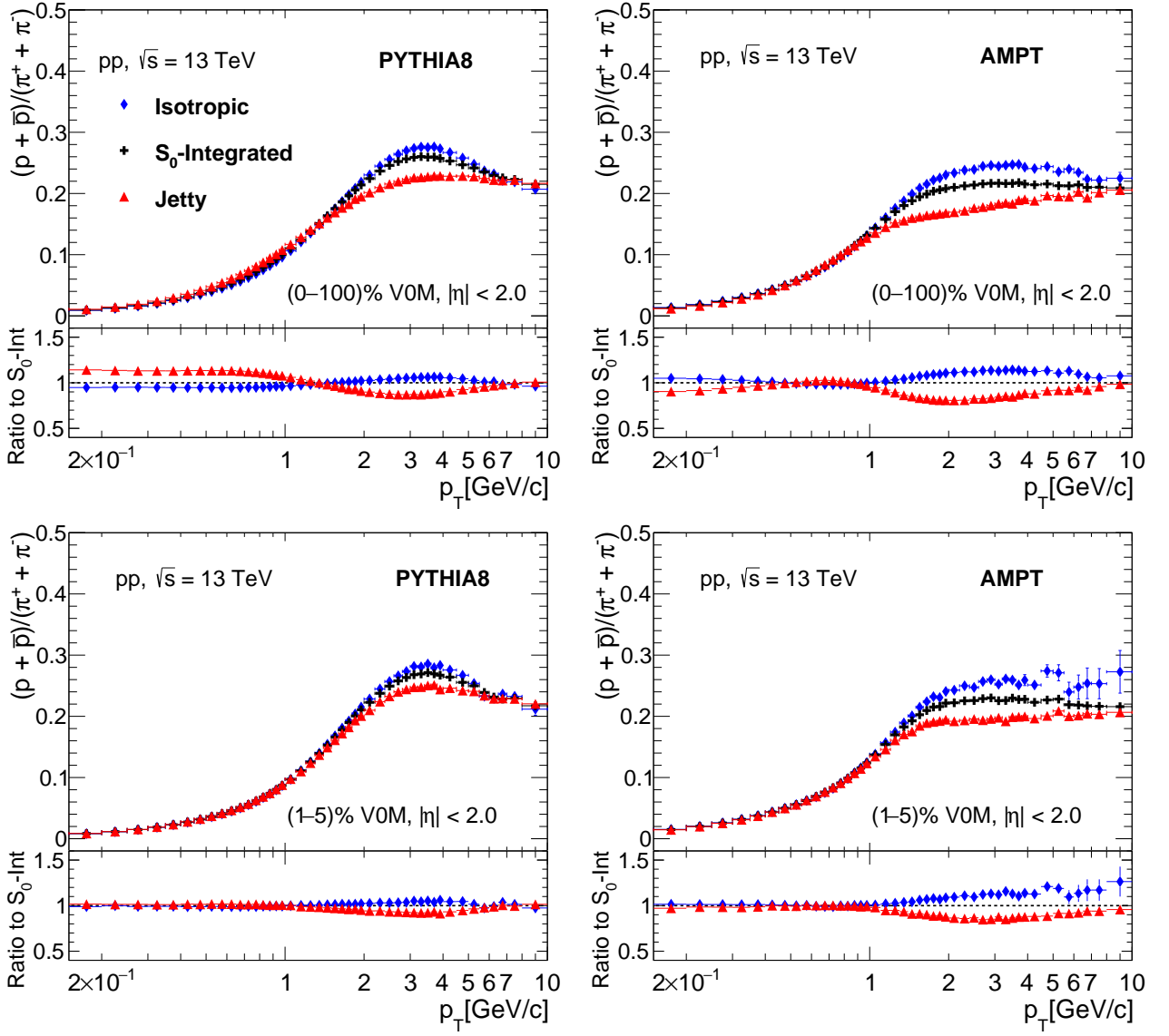


FIG. 5. (Color online) Proton-to-pion ratio as a function of transverse momentum at $|\eta| < 2.0$ for different sphericity bins for (0 – 100)% (top) and (1 – 5)% (bottom) V0M classes in pp collisions at $\sqrt{s} = 13$ TeV using PYTHIA8 (left) and AMPT (right).

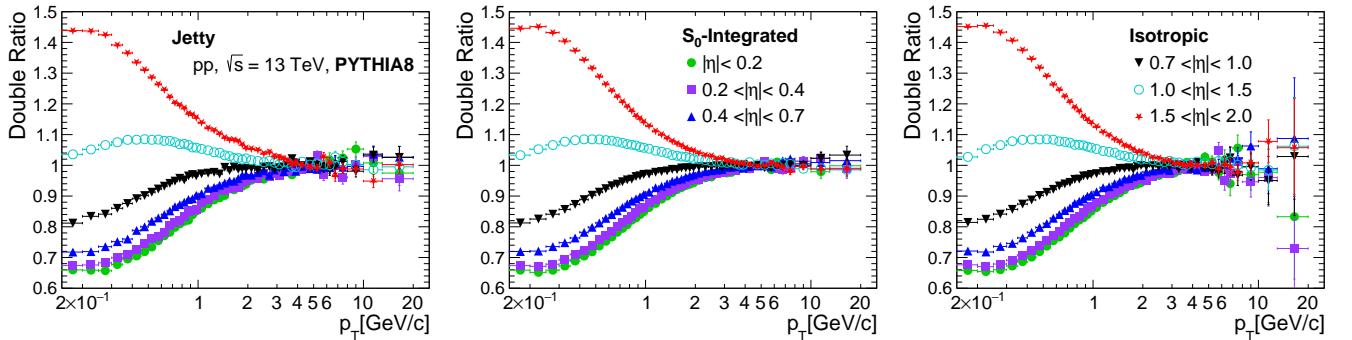


FIG. 6. (Color online) Proton-to-pion ratio normalized to their ratios in the pseudorapidity range, $|\eta| < 2.0$ as a function of transverse momentum for different pseudorapidity bins in pp collisions at $\sqrt{s} = 13$ TeV using PYTHIA8 for jetty (left), sphericity-integrated (middle) and isotropic (right) events. The results are shown for (0 – 100)% V0M class.

for the jetty events in (0 – 100)% V0M class, due to low N_{mpi} , p/π remains fairly flat in p_T and it means, jetty

events have a very tiny contribution towards radial flow-like effects. The case becomes interesting when the jetty events in the high-multiplicity pp collisions in (1–5)% V0M class show a peak around the same p_T value as the isotropic and S_0 -integrated events using PYTHIA8. The appearance of radial flow-like effects in the jetty events in high-multiplicity pp collisions can also be confirmed by comparing the bottom panels of both the multiplicity classes, where the ratio of the jetty to S_0 -integrated class approaches and stays close to unity for the high-multiplicity case. This is a testimony that with sphericity selection, we can separate the rare events which show an enhanced radial flow-like behaviour. At the same time, the jetty events show the presence of radial flow-like effects but only in the high-multiplicity events. Furthermore, similar behaviour of transverse sphericity dependence of p/π ratio can be seen in the AMPT model for the (0–100)% V0M class. Although here, the bump structure of p/π ratio in S_0 -integrated and jetty events can not be seen, the isotropic events show a visible bump-like structure. This indicates that, even if the flow-like effects are not visible in the minimum bias events, one can use transverse sphericity to identify the events with enhanced flow-like effects. In addition, one can notice that S_0 -integrated events for AMPT do not show a bump structure for (1–5)% V0M class in contrast to PYTHIA8, where a bump is clearly visible. However, one finds a finite bump structure for the isotropic events, which is clearly reflected in the bottom ratio plot. This indicates that in the AMPT model, although the charged particle multiplicity is not able to identify the flow-like events, the use of transverse sphericity makes a significant difference in the flow measurements.

Figure 6 shows the p/π yield double ratio as a function of transverse momentum in different rapidity windows for jetty, S_0 -integrated and isotropic events in (0–100)% V0M class. The double ratio is defined as,

$$\text{Double Ratio} = \frac{\left((p + \bar{p}) / (\pi^+ + \pi^-) \right)_{|\eta - \text{cut}}}{\left((p + \bar{p}) / (\pi^+ + \pi^-) \right)_{|\eta| < 2.0}}. \quad (2)$$

Here, the numerator is normalized to the p/π yield in the entire pseudorapidity range, i.e. $|\eta| < 2.0$. The double p/π ratio as a function of p_T shows a significant dependence on pseudorapidity selection at low p_T for all sphericity classes. The double ratio shows about 40% suppression (enhancement) for $|\eta| < 0.2$ ($1.5 < |\eta| < 2.0$) selection for $p_T < 2.0$ GeV/ c . Thereafter, the double ratio approaches a similar value for all pseudorapidity cases, and beyond $p_T \simeq 2$ GeV/ c , it seems to be independent of the pseudorapidity selection.

The suppression and enhancement of the double ratios observed in Fig. 6 is related to the radial flow-like effects. As, in the presence of large N_{mpi} , the radial flow-like effects are enhanced and the bump of the p/π ratio shifts to higher- p_T as compared to a system having low

radial flow-like effects, the ratio of the p/π of the former to the latter would show a suppression at the low- p_T region. However, it is to be noted that, in the presence of regeneration effects, which are significantly high in heavy-ion collisions compared to the pp collisions, the behaviour of the double ratio for a radially boosted system may change. For a system with both regeneration and radial flow effects, we may observe a suppression at low p_T and an enhancement in the intermediate p_T region. However, in pp collisions, the regeneration effects are negligibly small. Thus, in Fig. 6, the suppression observed in the double ratio at the midrapidity indicates that the system at midrapidity exhibits stronger radial flow-like effects as compared to that at forward rapidity. This is an important finding as this behavior shows that the radial-flow-like feature, indicated by the bump-like structure in p/π ratio at $p_T \simeq 2 - 6$ GeV/ c , is mildly affected by the pseudorapidity selection. It is also interesting to note that the double ratios show a negligible sphericity dependence for a fixed pseudorapidity selection, indicating that the sphericity preserves the capability of finding rare events with enhanced radial flow-like effects, irrespective of pseudorapidity selection.

B. Partonic modification factor (R_{pp})

It has been observed by the ALICE experiment [76], that the self-normalized charged particle yields for $p_T > 4$ GeV/ c have a faster than linear increase when studied as a function of average mid-pseudorapidity multiplicity. This non-linearity in the high- p_T particle yields is understood as a consequence of an autocorrelation bias due to the estimation of both charged particle yields and the charged particle multiplicity for event selection in the same pseudorapidity region [77]. To reduce such autocorrelation biases, the classification of events has been performed using forward pseudorapidity charged-particle multiplicity, while the observable of interest is measured in a different pseudorapidity interval [78]. Based on PYTHIA8 simulations, the charged particle multiplicity measured in forward pseudorapidity is strongly correlated to the underlying MPI activity [22]. However, the autocorrelation bias is still observed [79], which affects the observables that aim to search for medium-modification and partonic energy loss in small collision systems [71]. Thus, transverse sphericity, a key event shape classifier, plays an important role in reducing the sensitivity to hard processes compared to classifiers based only on forward pseudorapidity charged-particle multiplicity estimation. As this section aims to study the partonic modification factor (R_{pp}), which is related to both radial flow and partonic energy loss, the choice of transverse sphericity as an event classifier is expected to reduce such autocorrelation biases.

Traditionally, one of the observables constructed to understand how particle production in heavy-ion collisions differs from the baseline proton-proton collisions is the

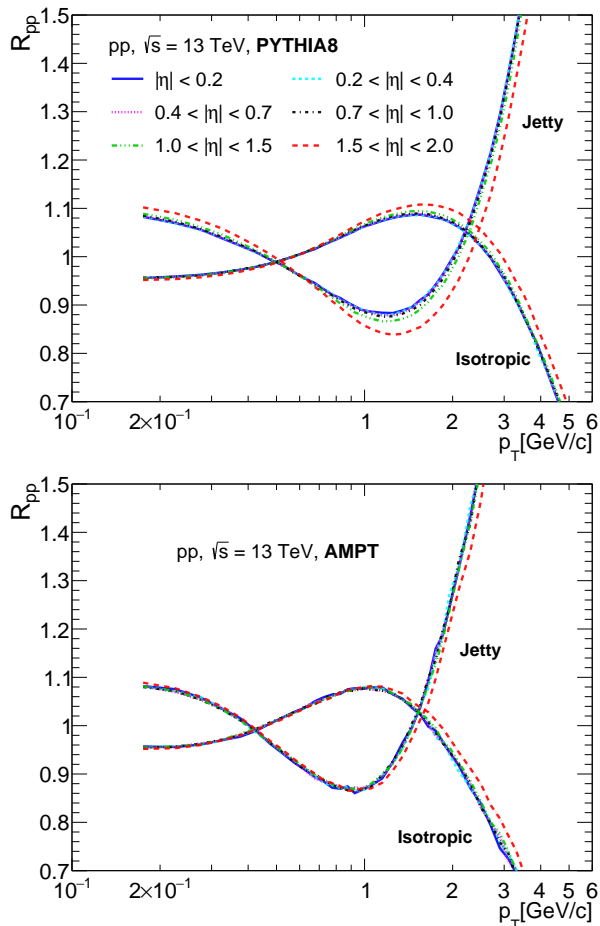


FIG. 7. (Color online) R_{pp} as a function of p_T for all charged hadrons for jetty and isotropic events within different pseudorapidity selections for (0–100)% V0M class in pp collisions at $\sqrt{s} = 13$ TeV using PYTHIA8 (top) and AMPT (bottom).

nuclear modification factor, R_{AA} . It is defined as the ratio of yield in heavy-ion collisions (A–A) to that of the yield in pp collisions normalized by the average number of binary collisions [40, 74].

$$R_{AA} = \frac{1}{\langle N_{\text{coll}} \rangle} \frac{d^2 N_{AA}/d\eta dp_T}{d^2 N_{pp}/d\eta dp_T}, \quad (3)$$

where the numerator is the p_T spectra in heavy-ion collisions while the denominator is the scaled p_T spectra in pp collisions by the total number of average binary pp collisions in a single A–A collision. In the absence of QGP medium formation, the yield in a single A–A collision is expected to be simply a linear superposition of the yield in the pp collisions times the number of binary pp collisions in a single A–A collision. This gives rise to the condition of $R_{AA} = 1$, suggesting no medium effect. $R_{AA} < 1$ ($R_{AA} > 1$) for identified particles indicates a suppression (enhancement) of hadrons which can be attributed to the presence of QGP medium. In addition, R_{AA} can also be affected by the cold nuclear matter ef-

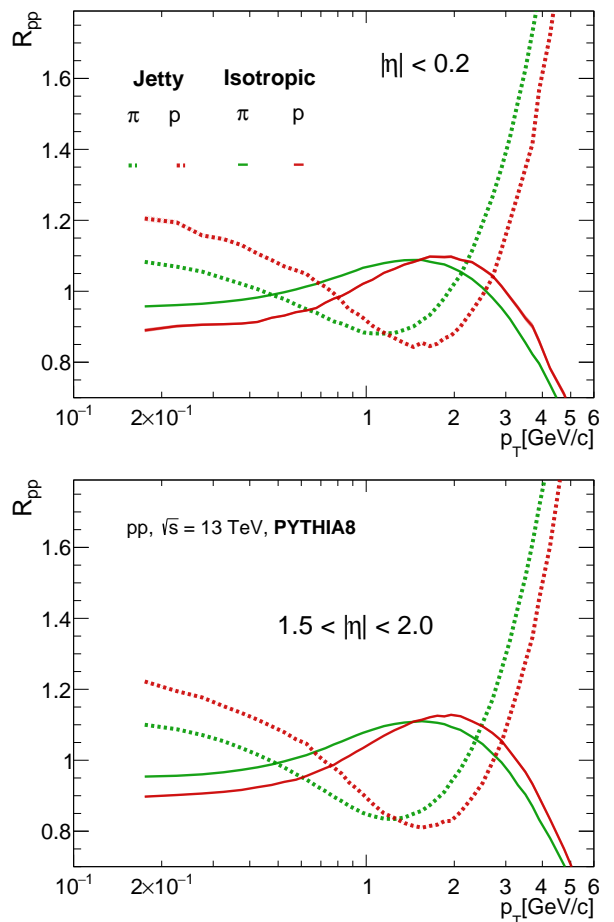


FIG. 8. (Color online) R_{pp} as a function of p_T for pions and protons for jetty and isotropic events in extreme η classes i.e. $|\eta| < 0.2$ (top) and $1.5 < |\eta| < 2.0$ (bottom) for (0–100)% V0M class in pp collisions at $\sqrt{s} = 13$ TeV using PYTHIA8.

fects [80, 81]. This includes initial state effects such as the modification of the parton distribution functions of the colliding nuclei with respect to the protons [82].

Since in our study, the system under focus is a proton-proton collision system and as the baseline used in the definition of nuclear modification factor is also a pp collision system, there is a requirement to redefine the modification factor accordingly. In Ref. [23], the authors have introduced a quantity motivated from R_{AA} , i.e., R_{pp} . We refer to this quantity as partonic modification factor. This is defined as the normalized ratio of the yield of all charged particles in a specific spherocity class and a particular pseudorapidity bin to their yield in the same pseudorapidity bin for S_0 -integrated events.

$$R_{pp} = \left. \frac{d^2 N_{\text{ch}}^{S_0} / \langle N_{\text{ch}}^{S_0} \rangle d\eta dp_T}{d^2 N_{\text{ch}}^{\text{MB}} / \langle N_{\text{ch}}^{\text{MB}} \rangle d\eta dp_T} \right|_{\eta} \quad (4)$$

Analogous to the $1/\langle N_{\text{coll}} \rangle$ in R_{AA} , here we normalize the yields with respect to the average charged-particle

multiplicity in the corresponding sphericity event class i.e. the normalization constant used for scaling here is $\langle N_{\text{ch}}^{\text{MB}} \rangle / \langle N_{\text{ch}}^{S_0} \rangle$.

Figure 7 shows R_{pp} as a function of p_{T} for isotropic and jetty events in different pseudorapidity regions in pp collisions at $\sqrt{s} = 13$ TeV using PYTHIA8 (top) and AMPT (bottom). As can be seen in Fig. 7 using both AMPT and PYTHIA8 models, R_{pp} for jetty events has initially, a decreasing trend in the intermediate p_{T} region after which it rapidly rises towards higher p_{T} domains. On the other hand, R_{pp} for isotropic events increases first and then drops, showing a suppression trend. This behavior is very similar when one studies R_{pp} as a function of p_{T} for a different N_{mpi} selections as shown in Ref. [23]. Here, the dip (bump) structure at the intermediate p_{T} followed by the enhancement (suppression) structure of R_{pp} at high- p_{T} are observed for a small (large) value of N_{mpi} [23]. This dip (bump) structure at the intermediate p_{T} mimics a small (large) radially boosted system compared to the minimum-bias events [23]. Using transverse sphericity as an event shape classifier, as shown in Fig. 7, we can extract similar features of R_{pp} with N_{mpi} selections. However, these enhancement and suppression trends in the yields for jetty and isotropic events, as shown in Fig. 7, have a mild dependence on pseudorapidity. For the forward pseudorapidity range, the enhancement and suppression are steeper compared to the mid-pseudorapidity region. In addition, both PYTHIA8 and AMPT models show similar behaviour of R_{pp} on transverse sphericity selection. However, one finds a larger dependence of pseudorapidity selection on R_{pp} using PYTHIA8 as compared to AMPT.

Figure 8 shows R_{pp} as a function of p_{T} for pions and protons for jetty and isotropic events in extreme η classes i.e. $|\eta| < 0.2$ and $1.5 < |\eta| < 2.0$ in pp collisions at $\sqrt{s} = 13$ TeV using PYTHIA8. A similar behavior is observed for both pions and protons as seen in Fig. 7. However, the key point to note from Fig. 8 is that a significant mass-dependent shift of peak position of enhancement and suppression at intermediate- p_{T} is observed for jetty and isotropic events, respectively. This mass dependence of the shift in the peak positions of R_{pp} is attributed to the color reconnection mechanism in PYTHIA8 and is seen as radial flow-like effect, where the heavier particles are largely boosted in presence of CR as compared to lighter particles, thus shifting the peak positions to higher p_{T} for the heavier particles [21].

C. Mean transverse momentum

Figure 9 shows $\langle p_{\text{T}} \rangle$ as a function of charged particle density for the jetty (left), S_0 -integrated (middle) and isotropic (right) events estimated in different regions of pseudorapidity in pp collisions at $\sqrt{s} = 13$ TeV from PYTHIA8. The $\langle p_{\text{T}} \rangle$ is calculated in the region $0.15 < p_{\text{T}} < 10$ GeV/ c . For all pseudorapidity selections, the $\langle p_{\text{T}} \rangle$ increases with $\langle dN_{\text{ch}}/d\eta \rangle$. This en-

hancement of $\langle p_{\text{T}} \rangle$ with multiplicity follows a similar trend as observed in Pb–Pb collisions and can be attributed to higher N_{mpi} which leads to higher radial flow-like effects with an increase in the charged particle density [83]. Here, one observes significant pseudorapidity dependence of $\langle p_{\text{T}} \rangle$. The value of $\langle p_{\text{T}} \rangle$ decreases with increased pseudorapidity. Since the mid-pseudorapidity regions, where the gluons dominate the particle production, are denser compared to forward pseudorapidities where the particle production is dominated by fragmentation and hadronic decays, the particle production is less favored at higher pseudorapidities compared to the midrapidities [84]. Thus, due to large parton density at the mid-rapidity, the probability of color reconnection of two independent partons becomes larger, and as a consequence, larger radial flow-like effects are observed. In addition, the expansion of the created partons in the longitudinal direction (forward- η) is faster than in the mid-pseudorapidity region. A faster longitudinal expansion would reduce the time for color reconnection of created partons. Thus the radial flow-like effects are diminished in forward-pseudorapidity [40]. The $\langle p_{\text{T}} \rangle$ is also found to show sphericity dependence, where $\langle p_{\text{T}} \rangle$ is higher for jetty events compared to the isotropic events throughout all pseudorapidity bins. The observed higher value of $\langle p_{\text{T}} \rangle$ for the jetty events is because of contribution due to the domination of jets.

To understand the pseudorapidity dependence of $\langle p_{\text{T}} \rangle$ in greater detail, in Fig. 10, $\langle p_{\text{T}} \rangle$ as a function of charged particle density for pions ($\pi^+ + \pi^-$), kaons ($K^+ + K^-$) and protons ($p + \bar{p}$) is studied for the jetty, S_0 -integrated and isotropic events in the extreme pseudorapidity selections in pp collisions at $\sqrt{s} = 13$ TeV using PYTHIA8. As the CR leads to a larger boost to heavier particles [21], a clear mass ordering is observed where $\langle p_{\text{T}} \rangle$ is more for protons than kaons and the least for pions. As expected from the trends observed in Fig. 9, at mid-pseudorapidity, the hadrons show a significant enhancement in $\langle p_{\text{T}} \rangle$ than that of forward-pseudorapidity hadrons. This drop of $\langle p_{\text{T}} \rangle$ from mid to forward pseudorapidity, with a more pronounced effect on heavier hadrons, once again reflects the diminishing nature of radial flow-like effects towards higher pseudorapidities. The observed pseudorapidity dependence of $\langle p_{\text{T}} \rangle$ in Fig. 10 is consistent with experimental observations in Cu–Cu collisions as shown in Ref. [40].

D. Kinetic freezeout parameters

The space-time evolution in ultra-relativistic collisions involves several phases. The traditional heavy-ion picture assumes the pre-equilibrium phase, the QGP phase, the mixed phase, the chemical freeze-out, the hadron gas phase, and finally, the kinetic freeze-out phase. The effect of radial flow thus migrates from the partonic QGP phase to the hadron gas phase and survives till the kinetic freeze-out giving a boost to the produced hadrons.

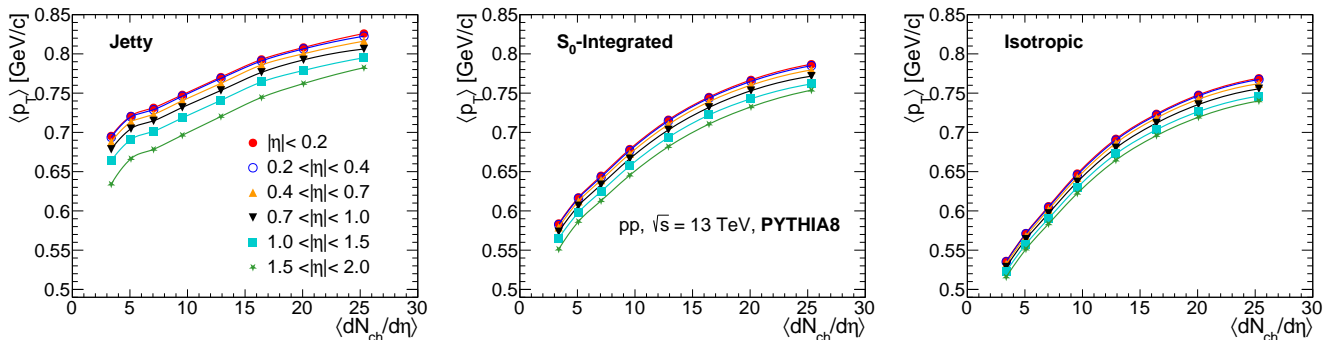


FIG. 9. (Color online) $\langle p_T \rangle$ versus $\langle dN_{ch}/d\eta \rangle$ as a function of pseudorapidity for jetty, S_0 -integrated and isotropic events in pp collisions at $\sqrt{s} = 13$ TeV using PYTHIA8.

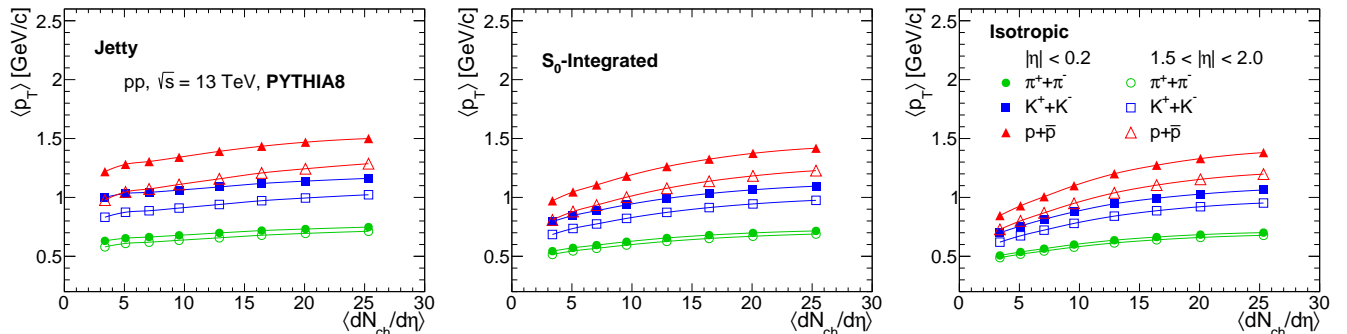


FIG. 10. (Color online) $\langle p_T \rangle$ versus $\langle dN_{ch}/d\eta \rangle$ for pions, kaons and protons as a function of extreme pseudorapidity classes for jetty, S_0 -integrated and isotropic events in pp collisions at $\sqrt{s} = 13$ TeV using PYTHIA8.

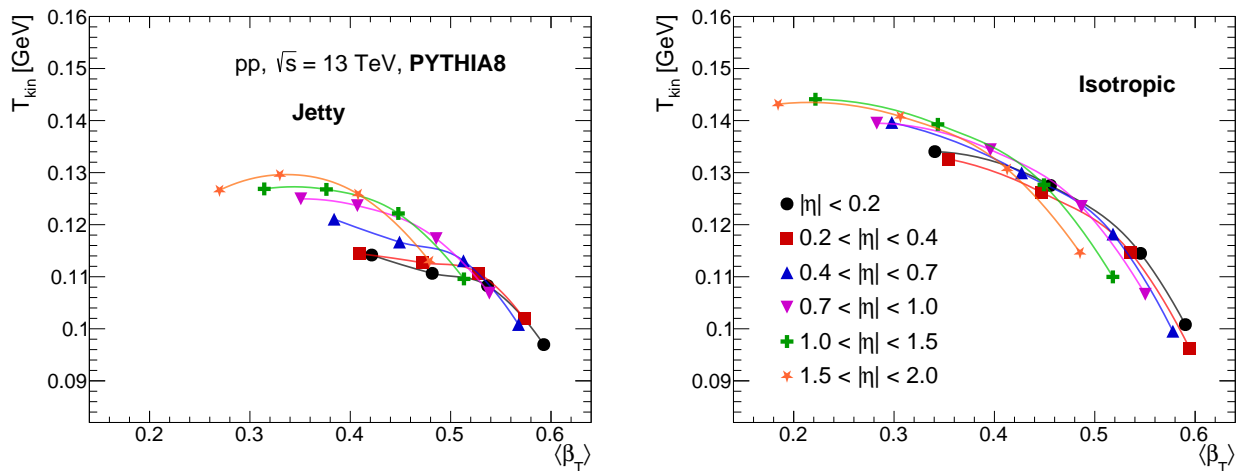


FIG. 11. (Color online) Kinetic freeze-out temperature versus mean transverse radial flow velocity as a function of pseudorapidity for jetty (left) and isotropic (right) events from the simultaneous blastwave fitting of the p_T spectra of protons, kaons, and pions in pp collisions at $\sqrt{s} = 13$ TeV using PYTHIA8.

This results in the enhancement of the expansion velocity of the hadronic system. This expansion velocity is imprinted in the transverse momentum spectra of the produced hadrons. As the transverse momentum spectra of identified hadrons obtained using PYTHIA8 exhibit flow-like effects which are traced back to CR and MPI,

it will be interesting to study the mean transverse expansion velocity ($\langle \beta_T \rangle$) and kinetic freeze-out temperature (T_{kin}). One can extract $\langle \beta_T \rangle$ along with T_{kin} by a simultaneous fitting of the Boltzmann-Gibbs blastwave (BGBW) function to the identified particles' transverse momentum spectra measured after the kinetic freeze-out.

The BGBW function at midrapidity is given by the following expression [40, 85]:

$$\left. \frac{d^2 N}{dp_T dy} \right|_{y=0} = C p_T m_T \int_0^{R_0} \left[r D(r) dr \times K_1 \left(\frac{m_T \cosh \rho}{T_{\text{kin}}} \right) I_0 \left(\frac{p_T \sinh \rho}{T_{\text{kin}}} \right) \right], \quad (5)$$

where $K_1 \left(\frac{m_T \cosh \rho}{T_{\text{kin}}} \right)$ and $I_0 \left(\frac{p_T \sinh \rho}{T_{\text{kin}}} \right)$ are modified Bessel's functions, which are given by,

$$K_1 \left(\frac{m_T \cosh \rho}{T_{\text{kin}}} \right) = \int_0^\infty \cosh y \exp \left(- \frac{m_T \cosh y \cosh \rho}{T_{\text{kin}}} \right) dy, \quad (6)$$

$$I_0 \left(\frac{p_T \sinh \rho}{T_{\text{kin}}} \right) = \frac{1}{2\pi} \int_0^{2\pi} \exp \left(\frac{p_T \sinh \rho \cos \phi}{T_{\text{kin}}} \right) d\phi, \quad (7)$$

where, $\rho = \tanh^{-1} \beta_T$ and $\beta_T = \beta_s \xi^n$ [85–88]. β_T is called radial flow, β_s is the maximum surface velocity, $\xi = (r/R_0)$ with r being the radial distance and R_0 the maximum radius of the source at freeze-out. $D(r)$ is the nuclear density profile; in our study, we have considered $D(r) = 1$ for $r < R_0$ and $D(r) = 0$ for $r > R_0$, i.e., hard sphere profile. In this model, the particles closer to the center of the fireball are assumed to move slower than the ones at the edges. The mean transverse velocity is given by [89],

$$\langle \beta_T \rangle = \frac{\int \beta_s \xi^n \xi d\xi}{\int \xi d\xi} = \left(\frac{2}{2+n} \right) \beta_s. \quad (8)$$

In Eq. 5, the modified Bessel's function comes as a consequence of the integration from $-\infty$ to $+\infty$ over pseudorapidity η , assuming boost invariance. However, as one goes towards the forward rapidity, the condition of boost invariance is not valid. Thus, the modified Bessel's function should be replaced by an integral, i.e., $g(z)$ for $z = m_T \cosh \rho / T_{\text{kin}}$ over a finite range of η , defined as follows [40].

$$g(z) = \int_{\eta_{\text{min}}}^{\eta_{\text{max}}} \cosh(\eta - y) e^{-z \cosh(\eta - y)} d\eta \quad (9)$$

Now, the substitution of Eq. 9 in Eq. 5 modifies as follows:

$$\left. \frac{d^2 N}{dp_T dy} \right|_{y=0} = C p_T m_T \int_0^{R_0} \left[r D(r) dr \times g \left(\frac{m_T \cosh \rho}{T_{\text{kin}}} \right) I_0 \left(\frac{p_T \sinh \rho}{T_{\text{kin}}} \right) \right] \quad (10)$$

Using Eq. 10, one can perform the simultaneous fitting to the transverse momentum spectra of pions ($\pi^+ + \pi^-$),

kaons ($K^+ + K^-$) and protons ($p + \bar{p}$). In Eq. 9, the value of y is chosen to be a pseudorapidity which lies exactly in the center of the polar angles corresponding to η_{min} and η_{max} . We use the similar fitting range from Ref. [28], i.e., $0.5 < p_T < 1$ GeV/c for pions, $0.3 < p_T < 1.5$ GeV/c for kaons and $0.8 < p_T < 2.0$ GeV/c for protons. The values obtained from fitting for $\langle \beta_T \rangle$ and T_{kin} as well as the corresponding χ^2/NDF values are tabulated in Tab. III. Kinetic freeze-out temperature (T_{kin}) versus mean transverse radial flow velocity ($\langle \beta_T \rangle$) as a function of transverse sphericity for two extreme pseudorapidity selections are plotted in Fig. 11. T_{kin} and $\langle \beta_T \rangle$ are found to be multiplicity dependent. Higher multiplicity classes show increased $\langle \beta_T \rangle$ and decreased T_{kin} which ought to be due to the longer time it would require to reach the freeze-out [45]. In addition, for a given class of transverse sphericity, because of the higher particle density at the mid-pseudorapidity, the particles at mid-pseudorapidity show a higher value of $\langle \beta_T \rangle$ and lower value of T_{kin} compared to the particles at the forward-pseudorapidity. Furthermore, a mild sphericity dependence is observed for both $\langle \beta_T \rangle$ and T_{kin} . For the high multiplicity class, the results are consistent with Ref. [45] for Pb–Pb collisions at $\sqrt{s_{\text{NN}}} = 5.02$ TeV, i.e., the isotropic events possess higher value of $\langle \beta_T \rangle$ and lower T_{kin} compared to the jetty events. However, as one moves towards the lower multiplicity class, due to dominating effects from the initial hard scatterings and jet fragmentations, the jetty events acquire higher values of $\langle \beta_T \rangle$ and lower T_{kin} .

E. Transverse momentum crossing points

The p_T values where the p_T spectra for jetty events start to dominate over the isotropic events are referred to as the p_T crossing points (p_T^{cross}). These crossing points suggest that the production of hadrons is dominated by isotropic events in the low p_T and jetty events in the high p_T region [25]. Figure 12 shows p_T^{cross} for two extreme pseudorapidity selections studied as a function of mean charged particle multiplicity density ($\langle dN_{\text{ch}}/d\eta \rangle$) for pions, kaons and protons in pp collisions at $\sqrt{s} = 13$ TeV using PYTHIA8. As one can observe, the crossing of p_T spectra of isotropic and jetty events has a clear multiplicity dependence, and the crossing point shifts towards higher p_T with increasing multiplicity. This would imply that the soft particle production in high multiplicity collisions lasts to higher values in p_T compared to low multiplicity events.

In Fig. 12, we also see a mass dependence where shifting of p_T crossing points to higher p_T is more for protons than kaons followed by pions, and this could be attributed to a flow-like behaviour caused by CR. This mass ordering is observed in all pseudorapidity windows, with the mass dependence becoming clearer only for high multiplicity classes. As discussed in earlier sections, CR with a larger N_{mpi} causes the transverse momentum of heavier particles to suffer a higher degree of broadening

η class	VOM Percentile	Isotropic			Jetty		
		$\langle\beta_T\rangle$	T_{kin} [GeV]	χ^2/NDF	$\langle\beta_T\rangle$	T_{kin} [GeV]	χ^2/NDF
$ \eta < 0.2$	0-1	0.590 ± 0.010	0.101 ± 0.007	0.547	0.593 ± 0.008	0.097 ± 0.005	0.833
	10-20	0.546 ± 0.013	0.114 ± 0.006	0.674	0.537 ± 0.009	0.108 ± 0.004	1.049
	30-40	0.456 ± 0.024	0.128 ± 0.008	1.260	0.482 ± 0.014	0.111 ± 0.006	0.833
	50-70	0.341 ± 0.042	0.134 ± 0.009	1.640	0.421 ± 0.018	0.114 ± 0.006	1.196
$0.2 < \eta < 0.4$	0-1	0.595 ± 0.010	0.096 ± 0.007	0.528	0.573 ± 0.012	0.102 ± 0.009	0.539
	10-20	0.535 ± 0.013	0.115 ± 0.006	0.674	0.528 ± 0.010	0.111 ± 0.006	1.127
	30-40	0.447 ± 0.024	0.126 ± 0.008	0.909	0.472 ± 0.012	0.113 ± 0.005	1.321
	50-70	0.355 ± 0.038	0.133 ± 0.009	1.678	0.409 ± 0.017	0.114 ± 0.006	2.059
$0.4 < \eta < 0.7$	0-1	0.578 ± 0.013	0.100 ± 0.008	0.307	0.568 ± 0.012	0.101 ± 0.008	0.475
	10-20	0.518 ± 0.014	0.118 ± 0.007	0.525	0.513 ± 0.014	0.113 ± 0.007	0.546
	30-40	0.427 ± 0.027	0.130 ± 0.009	1.082	0.449 ± 0.017	0.117 ± 0.007	0.848
	50-70	0.298 ± 0.040	0.140 ± 0.008	1.463	0.384 ± 0.019	0.121 ± 0.006	0.880
$0.7 < \eta < 1.0$	0-1	0.550 ± 0.015	0.107 ± 0.009	0.275	0.539 ± 0.014	0.107 ± 0.008	0.664
	10-20	0.487 ± 0.015	0.124 ± 0.006	0.568	0.486 ± 0.015	0.117 ± 0.007	0.459
	30-40	0.396 ± 0.028	0.134 ± 0.008	0.851	0.407 ± 0.018	0.124 ± 0.006	0.631
	50-70	0.283 ± 0.037	0.140 ± 0.007	0.731	0.351 ± 0.023	0.125 ± 0.007	0.559
$1.0 < \eta < 1.5$	0-1	0.222 ± 0.021	0.144 ± 0.004	1.936	0.314 ± 0.017	0.127 ± 0.005	0.733
	10-20	0.344 ± 0.019	0.139 ± 0.005	1.236	0.376 ± 0.014	0.127 ± 0.005	0.900
	30-40	0.449 ± 0.012	0.128 ± 0.005	0.782	0.448 ± 0.012	0.122 ± 0.005	0.696
	50-70	0.518 ± 0.009	0.110 ± 0.005	0.527	0.513 ± 0.008	0.110 ± 0.004	0.542
$1.5 < \eta < 2.0$	0-1	0.485 ± 0.010	0.115 ± 0.005	0.515	0.479 ± 0.010	0.113 ± 0.005	0.616
	10-20	0.413 ± 0.013	0.131 ± 0.005	0.811	0.408 ± 0.012	0.126 ± 0.005	0.745
	30-40	0.306 ± 0.017	0.141 ± 0.004	1.322	0.330 ± 0.014	0.130 ± 0.004	0.856
	50-70	0.184 ± 0.026	0.143 ± 0.004	1.941	0.270 ± 0.014	0.127 ± 0.003	1.327

TABLE III. Kinetic freeze-out temperature (T_{kin}), mean transverse radial flow velocity ($\langle\beta_T\rangle$) and χ^2/NDF values obtained from a simultaneous fit of identified charged particles' p_T spectra with Boltzmann-Gibbs blastwave function as a function of multiplicity, pseudorapidity and transverse sphericity classes in pp collisions at $\sqrt{s} = 13$ TeV from PYTHIA8.

compared to the lighter particles. This effect shifts the crossing point to higher values for massive particles compared to the light mass particles. Due to low N_{mpi} for a lower multiplicity class, the broadening of p_T -spectra is small and the crossing points for different particles are indistinguishable. As one moves towards the higher multiplicity class, the radial flow-like effects from CR shifts the crossing point to a higher p_T value for heavier particles, leading to a clear distinction between the crossing points of different masses. However, one does not observe any pseudorapidity dependence on the crossing points within the uncertainties.

IV. SUMMARY

This study aims to explore the pseudorapidity and transverse sphericity dependence of radial flow-like effects in pp collisions at $\sqrt{s} = 13$ TeV using AMPT and a pQCD-inspired model PYTHIA8, which reproduces the

experimental spectra and flow-like signatures observed in experiments by implementing CR and MPI. Unlike the earlier definitions of sphericity in the pseudorapidity range $|\eta| < 0.8$, here, we redefine sphericity in the $|\eta| < 2.0$ region. With this modification in sphericity, we perform the differential studies of various observables that are known to be sensitive to the radial flow-like effects as a function of transverse sphericity, pseudorapidity (upto $|\eta| < 2.0$) and charged-particle multiplicity wherever possible. These observables include $\langle p_T \rangle$, particle ratios such as p/π , kinetic freezeout parameters such as T_{kin} and $\langle\beta_T\rangle$, partonic modification factor (R_{pp}) and the transverse momentum crossing points between the jetty and isotropic events. For selected observables, a comparative study using AMPT, a model based on kinetic-theory, is also performed. The findings are summarised below.

1. The mean number of multipartonic interactions has a direct correlation with the transverse sphericity.

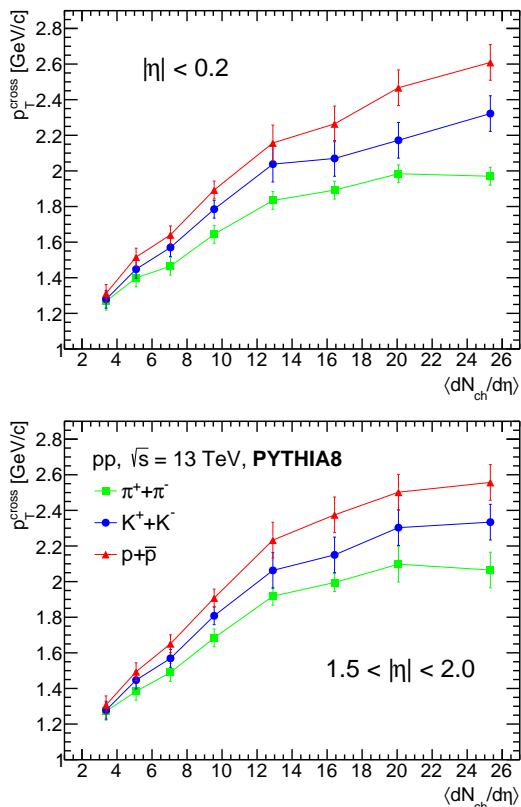


FIG. 12. (Color online) The crossing of the ratio of p_T spectra for isotropic and jetty events (p_T^{cross}) as a function of mean charged particle multiplicity density ($\langle dN_{\text{ch}}/d\eta \rangle$) for pions, kaons and protons in extreme pseudorapidity bins for pp collisions at $\sqrt{s} = 13$ TeV from PYTHIA8.

2. The p/π ratio as a function of p_T shows a peak-like structure at around 3 GeV/c where the sphericity dependence also becomes clearly distinct. Peak exhibited by isotropic events are more prominent than jetty events due to large N_{mpi} , which shows that the flow-like effects are enhanced in isotropic events.
3. At low to intermediate p_T , the suppression of the double ratio for the particles at mid-pseudorapidity signifies the presence of a large MPI activity as compared to the particles at the higher pseudorapidity regions, where an enhancement in the double ratio is observed.
4. Isotropic and jetty events show suppression and enhancement trends in partonic modification factor (R_{pp}) at higher p_T values, respectively. These effects are mildly enhanced at the central pseudorapidity region. R_{pp} shows a particle mass dependence, where the effects are enhanced for protons than pions.
5. The isotropic events show lower $\langle p_T \rangle$ than the jetty events due to large contributions from jets in the

jetty events. $\langle p_T \rangle$ increases with an increase in the charged particle multiplicity and towards the central pseudorapidity regions, indicating the effect from a large MPI activity leading to an enhanced radial flow-like scenario. The mass dependence of $\langle p_T \rangle$ for different rapidity regions indicates that the heavier mass particles receive a higher boost from CR compared to the lighter particles.

6. The kinetic freeze-out parameters viz. T_{kin} and $\langle \beta_T \rangle$ have clear multiplicity dependence, where an increase in multiplicity is associated with an enhanced flow velocity and a decreased kinetic freeze-out temperature. Particles at central pseudorapidity regions possess higher $\langle \beta_T \rangle$ and lower T_{kin} compared to the forward rapidity regions.
7. The transverse momentum crossing points have strong multiplicity dependence with p_T^{cross} shifting to higher values of p_T with increasing multiplicity. This indicates that the soft particle production lasts to higher values of p_T in high multiplicity events.
8. The dependence of p_T^{cross} on $\langle dN_{\text{ch}}/d\eta \rangle$ also shows a mass-ordering at all pseudorapidity bins and this becomes clearer at higher multiplicities. The observed shift in p_T^{cross} with multiplicity is higher for protons, followed by kaons and pions, which might also be pointing at the flow-like behaviour and can be attributed to CR.

In summary, the isotropic events are found to show significantly larger flow-like effects than the jetty events. At low multiplicities, several observables related to radial flow-like effects are prone to contributions from hard processes that are not part of MPI. In addition, the heavier particles are observed to gain a larger boost than the lighter particles from CR, which is consistent with hydrodynamic simulations. Furthermore, the pseudorapidity dependence of the radial flow-like effects, which is new in pp collisions, is explored by studying several observables. Experimentally observed radial flow signatures at midrapidity in high multiplicity pp collisions persist in the higher rapidities but with a reduced magnitude. This indicates that MPI activity has more significant effect on the hadrons produced at the mid-rapidity as compared to forward rapidity. The rapidity dependent effects are similar to the experimental results for Cu–Cu collisions [40]. As the ALICE detector at CERN has a planned upgrade to extend particle identification to $|\eta| < 4$, this study can motivate the experimentalists to cross-verify the findings with a clear physics goal in mind. In addition, comparing QGP signatures in pp collisions with those of heavy-ion collisions as a function of pseudorapidity may help the collider physics community understand the production of QGP droplets in pp collisions from a new angle.

DATA AVAILABILITY STATEMENT

This is a phenomenological paper with Monte-Carlo event generator data. In case the data are required by any of the readers, we shall provide the same upon request to the corresponding author.

ACKNOWLEDGEMENT

A.M.K.R. acknowledges the doctoral fellowships from the DST INSPIRE program of the Government of India. S.P. acknowledges the University Grants Commission (UGC), Government of India. The authors gratefully acknowledge the DAE-DST, Government of India funding under the mega-science project ‘‘Indian participation in the ALICE experiment at CERN’’ bearing Project No. SR/MF/PS-02/2021-IITI(E-37123).

APPENDIX

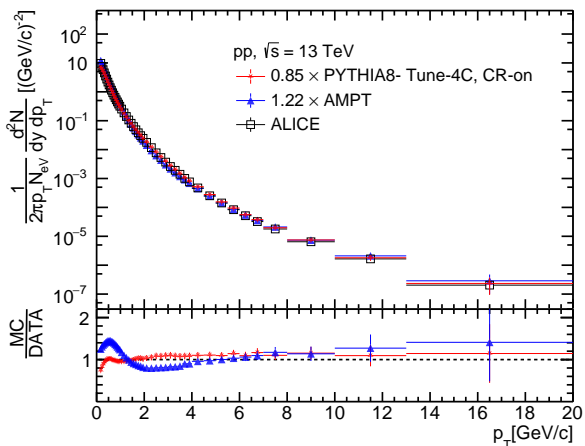


FIG. 13. (Color online) Comparison of PYTHIA8 generated data with AMPT and ALICE results [69] for transverse momentum spectra of all charged hadrons for minimum bias pp collisions at $\sqrt{s} = 13$ TeV.

In Fig. 14, we show p_T -differential proton-to-pion yield ratio as a function of $S_0(|\eta| < 0.8)$ for (0-100)% (upper) and (1-5)% (lower) V0M classes in pp collisions at

$\sqrt{s} = 13$ TeV using PYTHIA8. Here, one finds a similar qualitative behaviour of the proton-to-pion ratio as a function of p_T and transverse sphericity as shown in Fig. 5. However, in Fig. 14, a weaker sphericity dependence is found in comparison to Fig. 5 in both (0-100)% and (1-5)% V0M classes. This could result from a relatively weaker correlation of $S_0(|\eta| < 0.8)$ with $\langle N_{mpi} \rangle$, as shown in Fig. 3.

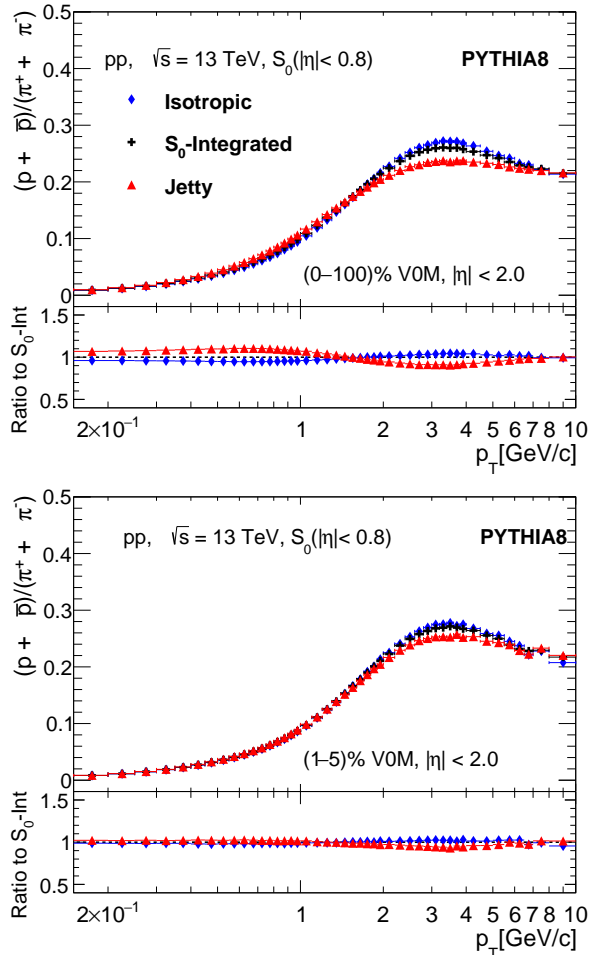


FIG. 14. (Color online) p_T -differential proton to pion yield ratio as a function of $S_0(|\eta| < 0.8)$ for (0-100)% (upper) and (1-5)% (lower) V0M classes in pp collisions at $\sqrt{s} = 13$ TeV using PYTHIA8.

[1] V. Khachatryan *et al.* [CMS], Phys. Rev. Lett. **116**, 172302 (2016).
 [2] B. B. Abelev *et al.* [ALICE], Phys. Lett. B **726**, 164 (2013).
 [3] J. Adam *et al.* [ALICE], Nature Phys. **13**, 535 (2017).
 [4] B. B. Abelev *et al.* [ALICE], Phys. Lett. B **728**, 25 (2014).

[5] J. Adam *et al.* [ALICE], Phys. Lett. B **760**, 720 (2016).
 [6] V. Khachatryan *et al.* [CMS], Phys. Lett. B **765**, 193(2017).
 [7] A. Kisiel, Phys. Rev. C **84**, 044913 (2011).
 [8] R. Preghenella [ALICE], J. Phys. Conf. Ser. **455**, 012009 (2013).
 [9] S. K. Das, P. Palni, J. Sannigrahi, J. e. Alam,

- C. W. Aung, Y. Bailung, D. Banerjee, G. G. Barnaföldi, S. C. Behera and P. P. Bhaduri, *et al.* Int. J. Mod. Phys. E **31**, 12 (2022).
- [10] J. Altmann, C. Andres, A. Andronic, F. Antinori, P. Antonioli, A. Beraudo, E. Berti, L. Bianchi, T. Boettcher and L. Capriotti, *et al.* Eur. Phys. J. C **84**, 421 (2024).
- [11] N. Mallick, R. Sahoo, S. Tripathy and A. Ortiz, J. Phys. G **48**, 045104 (2021).
- [12] N. Mallick, S. Tripathy and R. Sahoo, Eur. Phys. J. C **82**, 524 (2022).
- [13] N. Mallick, S. Prasad, A. N. Mishra, R. Sahoo and G. G. Barnaföldi, Phys. Rev. D **107**, 094001 (2023).
- [14] N. Mallick, S. Prasad, A. N. Mishra, R. Sahoo and G. G. Barnaföldi, Phys. Rev. D **105**, 114022 (2022).
- [15] S. Prasad, N. Mallick, S. Tripathy and R. Sahoo, Phys. Rev. D **107**, 074011 (2023).
- [16] N. Mallick, S. Tripathy, A. N. Mishra, S. Deb and R. Sahoo, Phys. Rev. D **103**, 094031 (2021).
- [17] D. Behera, N. Mallick, S. Tripathy, S. Prasad, A. N. Mishra and R. Sahoo, Eur. Phys. J. A **58**, 175 (2022).
- [18] D. Behera, S. Prasad, N. Mallick and R. Sahoo, Phys. Rev. D **108**, 054022 (2023).
- [19] T. Sjostrand, S. Mrenna and P. Z. Skands, Comput. Phys. Commun. **178**, 852 (2008).
- [20] A. Ortiz, G. Bencedi and H. Bello, J. Phys. G **44**, 065001 (2017).
- [21] A. Ortiz Velasquez, P. Christiansen, E. Cuautle Flores, I. Maldonado Cervantes and G. Paić, Phys. Rev. Lett. **111**, 042001 (2013).
- [22] A. Ortiz, A. Khuntia, O. Vázquez-Rueda, S. Tripathy, G. Bencedi, S. Prasad and F. Fan, Phys. Rev. D **107**, 076012 (2023).
- [23] A. Ortiz, A. Paz, J. D. Romo, S. Tripathy, E. A. Zepeda and I. Bautista, Phys. Rev. D **102**, 076014 (2020).
- [24] E. Cuautle, R. Jimenez, I. Maldonado, A. Ortiz, G. Paic and E. Perez, arXiv:1404.2372 [hep-ph].
- [25] A. Khuntia, S. Tripathy, A. Bisht and R. Sahoo, J. Phys. G **48**, 035102 (2021).
- [26] S. Deb, S. Tripathy, G. Sarwar, R. Sahoo and J. e. Alam, Eur. Phys. J. A **56**, 252 (2020).
- [27] A. Khatun, D. Thakur, S. Deb and R. Sahoo, J. Phys. G **47**, 055110 (2020).
- [28] A. Ortiz, G. Paic and E. Cuautle, Nucl. Phys. A **941**, 78 (2015).
- [29] G. P. Salam, Eur. Phys. J. C **67**, 637 (2010).
- [30] G. Bencedi [ALICE], Nucl. Phys. A **982**, 507 (2019)
- [31] A. Banfi, G. P. Salam and G. Zanderighi, JHEP **1006**, 038 (2010).
- [32] S. Tripathy, A. Bisht, R. Sahoo, A. Khuntia and M. P. Salvan, Adv. High Energy Phys. **2021**, 8822524 (2021).
- [33] S. Acharya *et al.* [ALICE], Eur. Phys. J. C **83**, 540 (2023).
- [34] V. Khachatryan *et al.* [CMS], Phys. Lett. B **768**, 103 (2017).
- [35] Z. B. Kang, I. Vitev and H. Xing, Phys. Lett. B **718**, 482 (2012).
- [36] P. Bozek, A. Bzdak and G. L. Ma, Phys. Lett. B **748**, 301 (2015).
- [37] B. Abelev *et al.* [ALICE], Phys. Rev. Lett. **110**, 082302 (2013).
- [38] S. Acharya *et al.* [ALICE], JHEP **11**, 013 (2018).
- [39] A. M. Sirunyan *et al.* [CMS], Phys. Rev. C **101**, 064906 (2020).
- [40] I. C. Arsene *et al.* [BRAHMS], Phys. Rev. C **94**, 014907 (2016).
- [41] B. B. Back *et al.* [PHOBOS], Phys. Rev. Lett. **91**, 072302 (2003).
- [42] A. Adare *et al.* [PHENIX], Phys. Rev. Lett. **121**, 222301 (2018).
- [43] A. Adare *et al.* [PHENIX], Phys. Rev. Lett. **114**, 192301 (2015).
- [44] C. Aidala *et al.* [PHENIX], Phys. Rev. C **95**, 034910 (2017).
- [45] S. Prasad, N. Mallick, D. Behera, R. Sahoo and S. Tripathy, Sci. Rep. **12**, 3917 (2022).
- [46] [ALICE], [arXiv:2211.02491 [physics.ins-det]].
- [47] B. Andersson, G. Gustafson, G. Ingelman and T. Sjostrand, Phys. Rept. **97**, 31 (1983).
- [48] R. Corke and T. Sjostrand, JHEP **03**, 032 (2011).
- [49] B. Zhang, C. M. Ko, B. A. Li and Z. w. Lin, [arXiv:nucl-th/9904075 [nucl-th]].
- [50] B. Zhang, C. M. Ko, B. A. Li and Z. W. Lin, Phys. Rev. C **61**, 067901 (2000).
- [51] B. Zhang, C. M. Ko, B. A. Li, Z. W. Lin and B. H. Sa, Phys. Rev. C **62**, 054905 (2000).
- [52] Z. W. Lin, S. Pal, C. M. Ko, B. A. Li and B. Zhang, Phys. Rev. C **64**, 011902 (2001).
- [53] Z. W. Lin, S. Pal, C. M. Ko, B. A. Li and B. Zhang, Nucl. Phys. A **698**, 375 (2002).
- [54] S. Pal, C. M. Ko and Z. W. Lin, Nucl. Phys. A **730**, 143 (2004).
- [55] Z. W. Lin and C. M. Ko, Phys. Rev. C **65**, 034904 (2002).
- [56] B. Zhang, C. M. Ko, B. A. Li, Z. W. Lin and S. Pal, Phys. Rev. C **65**, 054909 (2002).
- [57] S. Pal, C. M. Ko and Z. W. Lin, Nucl. Phys. A **707**, 525 (2002).
- [58] Z. W. Lin, C. M. Ko and S. Pal, Phys. Rev. Lett. **89**, 152301 (2002).
- [59] Z. W. Lin and C. M. Ko, Phys. Rev. C **68**, 054904 (2003).
- [60] Z. W. Lin and C. M. Ko, J. Phys. G **30**, S263 (2004).
- [61] X. N. Wang and M. Gyulassy, Phys. Rev. D **44**, 3501 (1991).
- [62] B. Zhang, Comput. Phys. Commun. **109**, 193 (1998).
- [63] Y. He and Z. W. Lin, Phys. Rev. C **96**, 014910 (2017).
- [64] B. Li, A. T. Sustich, B. Zhang and C. M. Ko, Int. J. Mod. Phys. E **10**, 267 (2001).
- [65] V. Greco, C. M. Ko and P. Levai, Phys. Rev. C **68**, 034904 (2003).
- [66] R. J. Fries, B. Muller, C. Nonaka and S. A. Bass, Phys. Rev. Lett. **90**, 202303 (2003).
- [67] R. J. Fries, B. Muller, C. Nonaka and S. A. Bass, Phys. Rev. C **68**, 044902 (2003).
- [68] S. Tripathy, S. De, M. Younus and R. Sahoo, Phys. Rev. C **98**, 064904 (2018).
- [69] J. Adam *et al.* [ALICE], Phys. Lett. B **753**, 319 (2016).
- [70] A. Nassirpour, EPJ Web Conf. **259**, 13005 (2022).
- [71] S. Acharya *et al.* [ALICE], Phys. Lett. B **843**, 137649 (2023).
- [72] S. Acharya *et al.* [ALICE], JHEP **05**, 229 (2024).
- [73] B. B. Abelev *et al.* [ALICE], Int. J. Mod. Phys. A **29**, 1430044 (2014).
- [74] S. Acharya *et al.* [ALICE], Phys. Rev. C **101**, 044907 (2020).
- [75] B. Abelev *et al.* [ALICE], Phys. Rev. C **88**, 044910 (2013).
- [76] S. Acharya *et al.* [ALICE], Eur. Phys. J. C **79**, 857 (2019).
- [77] S. G. Weber, A. Dubla, A. Andronic and A. Morsch, Eur.

- Phys. J. C **79**, 36 (2019).
- [78] S. Acharya *et al.* [ALICE], Phys. Rev. C **99**, 024906 (2019).
- [79] S. Acharya *et al.* [ALICE], Eur. Phys. J. C **80**, 693 (2020).
- [80] R. Aaij *et al.* [LHCb], Phys. Rev. Lett. **128**, 142004 (2022).
- [81] J. L. Albacete, F. Arleo, *et al.* Nucl. Phys. A **972**, 18 (2018).
- [82] K. J. Eskola, P. Paakkinen, H. Paukkunen and C. A. Salgado, Eur. Phys. J. C **77**, 163 (2017).
- [83] B. B. Abelev *et al.* [ALICE], Phys. Lett. B **727**, 371 (2013).
- [84] P. Sahoo, P. Pareek, S. K. Tiwari and R. Sahoo, Phys. Rev. C **99**, 044906 (2019).
- [85] E. Schnedermann, J. Sollfrank and U. W. Heinz, Phys. Rev. C **48**, 2462 (1993).
- [86] P. Huovinen, P. F. Kolb, U. W. Heinz, P. V. Ruuskanen and S. A. Voloshin, Phys. Lett. B **503**, 58 (2001).
- [87] P. Braun-Munzinger, J. Stachel, J. P. Wessels and N. Xu, Phys. Lett. B **344**, 43 (1995).
- [88] Z. Tang *et al.*, Chin. Phys. Lett. **30**, 031201 (2013).
- [89] K. Adcox *et al.* [PHENIX], Phys. Rev. C **69**, 024904 (2004).